

# Addressing the Elusive Polaronic Nature of Multiple Redox States in a $\pi$ -Conjugated Ladder-Type Polymer

Daniele Fazzi\* and Fabrizia Negri

Poly(benzimidazole–benzophenanthroline) (BBL) is a ladder-type conjugated polymer showing remarkable charge transport properties. Upon doping it displays various conductive regimes, leading to two insulator-to-conductor transitions. Such transitions are never fully characterized, limiting understanding of its charged states. Open issues are: i) the electron/hole polaron relaxations, ii) the structure–function relationships of multiple redox states and their connection with the conductive regimes, and iii) the role of protonation. Such knowledge-gaps are tackled via a comprehensive computational investigation of multiple redox species. Polarons show polyradicaloid character, as revealed by combining broken-symmetry density functional theory, fragment orbital density, and multireference analysis. Electron/hole polaron relaxations occur on the polymer chain, the former localizing on the benzophenanthroline moieties, the latter on the benzimidazole units. Modeling of multiple charged species, up to one electron per repeat unit (1 eru), reveals a complex scenario of quasidegenerate states each featuring different spin multiplicity. Four redox states are responsible for the BBL insulator-to-conductor transitions. The two high conductive states refer to the electron polaron (0.25 eru) and the redox species with 0.75 eru. The insulating regimes refer to the bipolaron (0.50 eru) and the redox state with 1 eru. Protonation is modeled, revealing polaron-like features in the spectroscopic properties.

## 1. Introduction

Ladder-type conjugated polymers (LCPs) belong to the class of high-performance organic functional materials, featuring enhanced mechanical, thermal, chemical, and optoelectronic

properties with respect to their nonladder systems.<sup>[1]</sup> The unique functionalities of LCPs can be traced back to their molecular structure, which consists of double strand chains connected by condensed  $\pi$ -conjugated units, resulting in a periodic sequence of elements that resembles the shape of a ladder.<sup>[2]</sup>

A consequence of such molecular architecture is the suppression of the dihedral angle linking two repeat units, thus leading to quasiflat systems showing high long-range order at the molecular scale. In comparison to classical conjugated polymers, LCPs show a lower intrachain torsional disorder, leading to a better  $\pi$ - $\pi$  stacking and densely packed nanostructures.<sup>[1a]</sup> Furthermore, planarity induces an extended  $\pi$ -electron delocalisation, providing small bandgap and optical gap, and an overall low structural and electronic entropy.<sup>[3]</sup>

Following such as simple as powerful structural design-rule a variety of LCPs were synthesised over the last decades. Examples dated back to 1960s are poly(benzimidazole–benzophenanthroline) (BBL)<sup>[4]</sup> and its derivative SBBL, polyquinoxaline (PQL), and poly(phenoxazine) (POL).<sup>[1a,5]</sup> After these pioneering works, new LCPs belonging to the family of ladder-type poly(p-phenylene) (LPPPs), poly(p-phenacene)s, poly(thioacenes), and D–A imide-derivatives, were recently proposed.<sup>[6]</sup>


Despite their promising structure–property functions, LCPs have never overtook both replaced traditional  $\pi$ -conjugated polymers as active materials for optoelectronic and energy saving applications. Reasons for that are related to issues encompassing i) few effective synthetic strategies to construct defect free LCPs, ii) poor solubility, iii) complex protonation states in aqueous media, and iv) unclear redox mechanisms occurring both in solutions and solid state.

Amongst LCPs, BBL is the most investigated and promising one. It was synthesized in 1966 aiming at producing polymer fibres with high mechanical and thermal stability properties.<sup>[4]</sup> Results were not promising and in 1982<sup>[7]</sup> Kim renewed the attention on BBL suggesting it as a candidate for polymeric materials with high mechanical, thermal, chemical, and electrical properties.<sup>[8]</sup> Kim was amongst the first one documenting chemical doping in BBL, finding a remarkable enhancement in the electrical conductivity ( $\sigma$ ) upon both oxidation and reduction. Both processes, increased  $\sigma$  of 12 orders of magnitude, from  $10^{-12}$  S cm<sup>-1</sup> (pristine) to 2 S cm<sup>-1</sup> (doped).<sup>[8,9]</sup>

Both processes, increased  $\sigma$  of 12 orders of magnitude, from  $10^{-12}$  S cm<sup>-1</sup> (pristine) to 2 S cm<sup>-1</sup> (doped).<sup>[8,9]</sup>

Dr. D. Fazzi  
Institut für Physikalische Chemie  
Department Chemie  
Universität zu Köln  
Luxemburger Str. 116 D-50939, Köln, Germany  
E-mail: dfazzi@uni-koeln.de

Prof. F. Negri  
Dipartimento di Chimica 'G. Ciamician'  
Università di Bologna  
Via F. Selmi, 2, Bologna 40126, Italy

 The ORCID identification number(s) for the author(s) of this article can be found under <https://doi.org/10.1002/aelm.202000786>.

© 2020 The Authors. Advanced Electronic Materials published by Wiley-VCH GmbH. This is an open access article under the terms of the Creative Commons Attribution License, which permits use, distribution and reproduction in any medium, provided the original work is properly cited.

The copyright line for this article was changed on 20 January 2021 after original online publication.

DOI: 10.1002/aelm.202000786

At the end of 1980s, Wilbourn and Murray explored the electrochemical doping of BBL in aqueous solutions and solid state films.<sup>[10]</sup> Despite a broad set of techniques, e.g., CV, coulometry, and spectroelectrochemistry, the complex redox behavior of BBL remained largely unclear. Difficulties arose in understanding the following aspects: i) the protonation state(s) and relative equilibrium in condensed phases, ii) the redox processes which lead to multiple CV peaks and to two conductive states showing high and low  $\sigma$  values (a factor of ten between the two), iii) the quantification of the amount of stored charge(s) per repeat units, and iv) the spectroscopic and charge transport properties of multiple redox species.

At the end of 1990s Sandreczki group<sup>[11]</sup> and Sariciftci group<sup>[12]</sup> were able to perform electron spin resonance and FT-IR spectroelectrochemistry experiments, getting insights into the multiple reduction processes of BBL. Contradicting conclusions however emerged, concerning the amount of consumed charge(s) per polymer unit during the doping processes, the assignments between the observed multiple redox states, and the two (high vs low) electrical conductive states.<sup>[13]</sup>

A plausible description was provided by Sariciftci and co-workers around 2000,<sup>[14]</sup> by coupling CV, FT-IR, and electrical conductivity measurements. In accordance to Wilbourn and Murray,<sup>[13]</sup> they found that the electrical conductivity of BBL varied by changing the potential during electrochemical reduction, showing two insulator-to-conductor transitions, thus leading to two conductive states with high (conductive state I:  $9 \times 10^3 \text{ S cm}^{-1}$  at  $-600 \text{ mV}$  in  $0.1 \text{ M Bu}_4\text{NClO}_4$ -acetonitrile electrolyte), and low (conductive state II:  $1.5 \times 10^3 \text{ S cm}^{-1}$  at  $-1000 \text{ mV}$ ) conductivity. As inferred by Sariciftci and co-workers,<sup>[14]</sup> the two insulator-to-conductor transitions referred to the presence of four reversible redox reactions (in contrast to Murray, who reported only two). Such redox species (named A, B, C, D) were assigned to two conductive and two insulating states, respectively. Sariciftci and co-workers proposed a multiple-charging reduction scheme in which the total number of consumed electron per repeat unit (eru) was measured as one, and the four redox species were classified as follows:<sup>[14]</sup> A, eru = 0.25, conductive state I; B, eru = 0.50, insulator state I; C, eru = 0.85, conductive state II; D, eru = 1, insulator state II. FT-IR spectra showed induced absorption vibration (IRAV) bands tentatively assigned to different negatively charged species, however insights into the structural, vibrational, and electronic properties of such hypothesized polaronic states were missing.

Despite such breakthrough in characterizing the complex redox behaviours of BBL, only phenomenological observations were reported, while fundamental understanding was lacking.

Given such multifaceted electrochemical and optical properties, BBL was broadly studied in the last two decades for different applications including pioneering works of Jenekhe and co-workers,<sup>[15]</sup> on electron transport (n-type) organic field effect transistors ( $\mu = 0.03\text{--}0.1 \text{ cm}^2 \text{ V}^{-1} \text{ s}^{-1}$ ),<sup>[16]</sup> heterojunction solar cells,<sup>[17]</sup> thermoelectric devices,<sup>[18]</sup> battery electrodes,<sup>[16c,19]</sup> and bipolar high conductive D–A polymer interfaces.<sup>[20]</sup>

For each application the role of multiredox states (involving either holes or electrons), and different protonated species (ubiquitously present in BBL, given its solubility in strong protonic acids) were never fully characterized nor understood.

Pioneering quantum-chemical calculations were reported in 1992 by Kim and co-workers.<sup>[21]</sup> They investigated the structural

and electronic properties of neutral and protonated BBL within the framework of semiempirical methods, however the approximated level of theory did not allow them neither to catch the underlying mechanisms, nor to explain the experimental data.

In 2016 Fabiano and co-workers reported the first joint experimental and computational investigation about BBL thermoelectric and polaronic properties.<sup>[18]</sup> Within the frame of density functional theory (DFT), they showed the presence of low-energy broken-symmetry unrestricted (BS-UDFT) solutions for a negatively charged state, leading to a spatially localized (electron) polaron over the ladder structure. In 2019, Zozoulenko and co-workers,<sup>[22]</sup> reported DFT calculations for multiple charged states of BBL, up to two electrons per repeat unit (2 eru). Despite Ghosh et al.<sup>[22]</sup> represent an attempt in modeling multiple negatively charged states of BBL, it does not document the underlying DFT instabilities in determining the charged electronic wavefunctions, therefore the claimed state energies, spin, and response properties should be revisited.

Recently, we extended the quantum-chemical investigation of single and double negatively charged states (electron, polaron, and bipolaron<sup>[23]</sup>) of BBL.<sup>[24]</sup> We confirmed that DFT leads to unstable solutions for the charged electronic wavefunction,<sup>[25]</sup> given the multiconfigurational character and electron correlation effects of charged states. We demonstrated how BS-UDFT might be an effective approach to overcome such issue, well describing the electron polaron/bipolaron localization in terms of spin densities and structural deformations,<sup>[26]</sup> and providing a correct assessment of the vibrational and electron transport properties in comparison to experimental data.

Notably, even though BBL has been experimentally investigated over the last two decades, fundamental physicochemical properties remain largely unsolved yet, limiting our basic understanding, therefore restricting potential improvements to the whole class of LCPs.

The central idea of our work is to fill such knowledge-gap by modeling the multicharged redox state properties of BBL. In particular, i) we extended our investigation from electron to hole charged species, showing their different structural and spin relaxations over the polymer chain, together with their polyradicaloid character. ii) We modeled multinegative charged states considering up to one electron per repeat unit (1 eru), providing insights into the charging mechanisms and conductive species present upon doping. iii) We predicted the structure–property relationships of protonated and protonated/reduced states, and ultimately, iv) we calculated the response properties of all redox species so far considered, computing their vibrational and electronic spectra, and comparing the results with experimental data.

We were able to provide a comprehensive understanding to the experiments, by assigning the spectroscopic features of multiple redox species underlying the two observed insulator-to-conductor transitions,<sup>[14]</sup> and by describing the role of protonated states in affecting the vibrational and electronic spectra of BBL. We found that the first high conductive state can be assigned to a polaron (0.25 eru), while the first insulating state is attributed to a bipolaron (0.50 eru). The two other states, bringing 0.75 and 1 eru, are related to the second conductive and insulating state, respectively. Protonated species show clear polaron-like features, detectable via IR and UV–vis spectroscopies as suggested by our computational predictions.

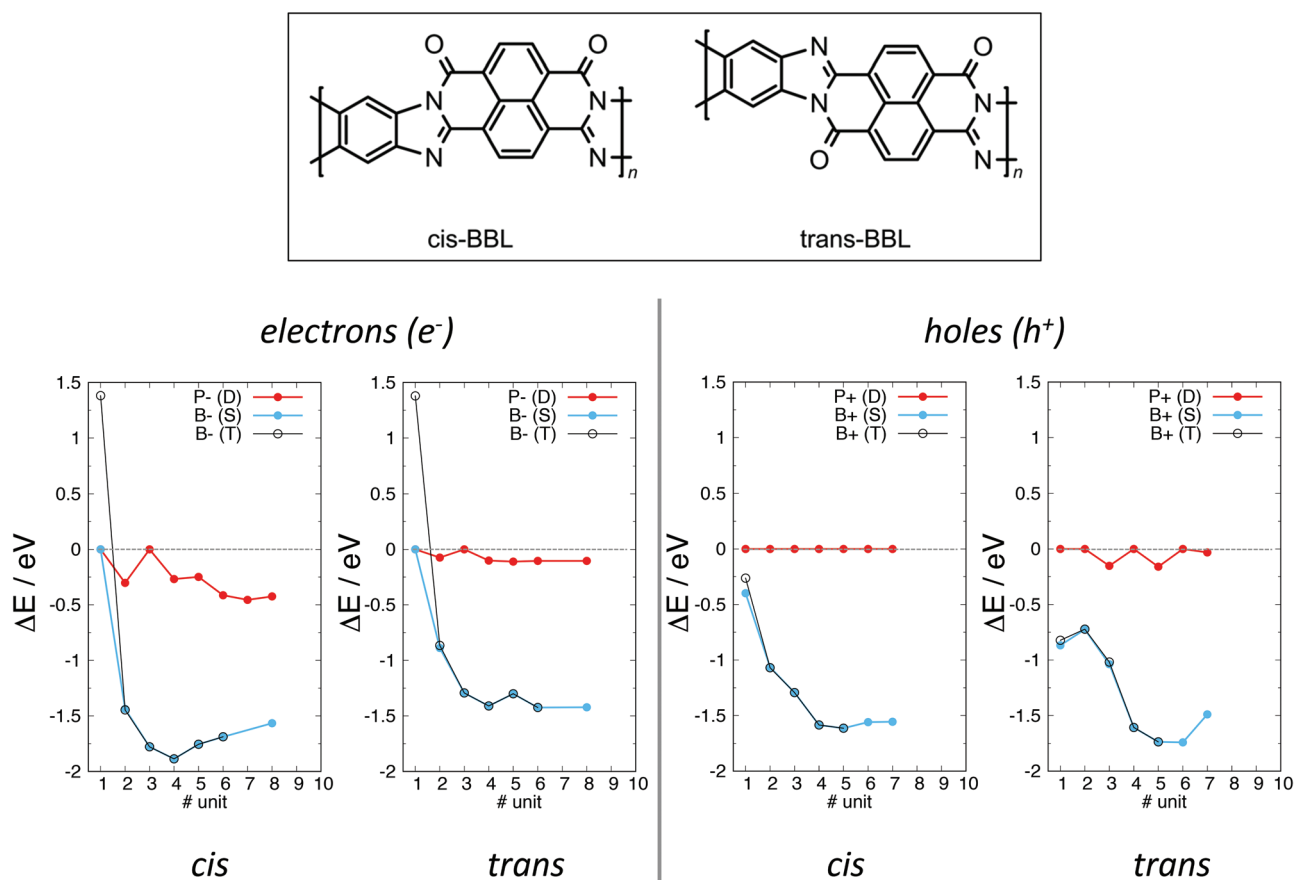


**Figure 1.** Top panel: chemical structures of *cis* and *trans* BBL conformers. Bottom panels: stabilization energy  $\Delta E$  (see definition in the main text) for polaron doublet P(D) (red), bipolaron singlet B(S) (blue), and triplet B(T) (black) states by changing the oligomer size  $n$  ( $n = \#$ number of unit, 1–8), for electron (left) and hole (right). DFT functional:  $\omega$ B97X-D, basis set: 6-31G\*. Negative energies refer to BS-UDFT calculations ( $P \pm (D)$ ,  $B \pm (S)$ ), or UDFT calculations ( $B \pm (T)$ ). Data for electrons are readapted from Ref. [24]. Reproduced with permission.<sup>[24]</sup> Copyright 2019, Royal Society of Chemistry.

Our study reconciles contradictory observations,<sup>[10,14,22]</sup> addressing fundamental questions, namely, i) what are the multiple-charging processes observed in BBL upon doping, ii) how much charge is stored per polymer repeat unit, iii) what are the polaronic species governing the high and low conductive states during the insulator-to-conductor transitions, iv) how electrons and holes relax over the polymer chain, and v) what are their main spectroscopic responses.

## 2. Results and Discussion

### 2.1. Electronic Structure of BBL Polarons and Bipolarons: Electron versus Hole

Aiming at a full understanding of the charging processing occurring in BBL (see chemical structure and conformers in **Figure 1**), we modeled a variety of electronic states differing by the total charge ( $q$ ) and spin state multiplicity. Charges were referred to be positive or negative, representing hole or electron doping, respectively. The electronic states for single ( $|q| = 1e$ ) and double ( $|q| = 2e$ ) charged species were named as: polaron –  $q = \pm 1e$  ( $P+$  hole,  $P-$  electron), state multiplicity doublet (D); bipolaron –  $q = \pm 2e$  ( $B+$ ,  $B-$ ), state multiplicities

singlet (S) or triplet (T). Multiple redox species, in analogy to the experimental data,<sup>[10,14]</sup> were investigated only for the case of electrons, namely:  $q = 3e^-$ , state multiplicities doublet (D) or quartet (Q), and  $q = 4e^-$ , state multiplicities singlet (S), triplet (T), quintet (Qui), and  $q = 5e^-$ , state multiplicities doublet (D), quartet (Q), and sextet (Sex) (see Supporting Information). For each electronic state, we optimized the structure and checked the stability of the DFT wavefunction. If an instability was found, both electronic and nuclear coordinates were then reoptimized at the broken symmetry (BS) UDFT level, as already reported in refs. [18 and 24a] specifically for BBL. For details concerning the theoretical background and broad applications of the BS formalisms to inorganic, organic, and hybrid compounds we refer the reader to ref. [24b-g]. Further computational details are given in the Supporting Information.

Figure 1 reports the positive versus negative polarons ( $P \pm (D)$  – red) and bipolarons ( $B \pm (S)$  – blue,  $B \pm (T)$  – black) stabilization energies ( $\Delta E$ ) for each BBL oligomer length (BBL1–8).  $\Delta E$  is defined as the energy difference between the BS-UDFT and the standard DFT solutions. For  $P \pm (D)$   $\Delta E$  is computed as  $\Delta E = E(\text{BS-UDFT}) - E(\text{UDFT})$ , for  $B \pm (S)$  as  $\Delta E = E(\text{BS-UDFT}) - E(\text{RDFT})$ , and for  $B \pm (T)$  as the energy difference between triplet and singlet states,  $\Delta E = E(T) - E(S)$ . As already discussed by Fazzi et al.,<sup>[24a]</sup> electron polaron  $P-(D)$  shows an instability the

longer is the BBL chain. Starting from BBL4, both *cis* and *trans* conformers show a BS-UDFT solution for P-(D), lower than the respective UDFT solution. For the case of bipolarons,<sup>[24a]</sup> the situation is more pronounced than polarons. The instability of the DFT for a singlet bipolaron (B-(S)) is found starting from BBL2, leading to  $\Delta E$  larger than 1 eV for long oligomers. The triplet bipolaron state (B-(T)) shows  $\Delta E$  very much similar to the singlet B-(S), differing for less than  $10^{-4}$  eV from the latter. The found BS solutions, recall for a multiconfigurational character<sup>[24b,c]</sup> and correlation effects of the electronic wavefunction<sup>[27]</sup> for BBL polarons and bipolarons.

We extended the quantum-chemical investigation to positively charged states, namely, hole polarons P+(D) and bipolarons B+(S), B+(T), as shown in Figure 1. For P+(D) *cis* conformers do not show wavefunction instability, while *trans* do show BS solutions for certain lengths (BBL3, 5, and 7). As for electrons, hole singlet bipolaron states B+(S) report wavefunction instability, leading to  $\Delta E$  larger than 1.5 eV for long oligomers. Contrary to electron bipolarons, hole B+(S) presents a BS solution at the monomer level (BBL1) already, with  $\Delta E = 0.5$  and 1 eV for *cis* and *trans*, respectively. This is a remarkable aspect, because it highlights the multireference (MR) and polyradicaloid character<sup>[28]</sup> of the double charged (bipolaron) hole-wavefunction.

In analogy to negatively charged species, the stabilization energies of hole bipolaron triplet states B+(T) are also reported in Figure 1, following the same trend as discussed for B-(T).

In general, the presence of low energy BS-UDFT solutions, regardless the nature of the charge, highlights a complex electronic structure scenario in which static electron correlation (SEC) and MR effects play relevant role.<sup>[29]</sup> Despite BS-UDFT is based on a single-determinant approach,<sup>[30]</sup> it has been demonstrated that it can qualitatively describe situations in which SEC<sup>[24b-g,31]</sup> and MR or polyradicaloid characters are predominant,<sup>[28,32]</sup> providing reasonable results in comparison to MR methods.<sup>[24b-g,33]</sup> Unquestionably, high-level quantum chemical methods, such as quantum Monte Carlo (QMC) techniques combined with the resonating-valence-bond (RVB) theory,<sup>[34]</sup> would provide a better description of the electronic structure and correlation effects as compared to BS-UDFT or wavefunction MR techniques, however such approaches are still too demanding to be applied for polymeric materials. A successful attempt was recently documented for the case of acenes, where MR effects were addressed via QMC/RVB,<sup>[30]</sup> showing that the diradicaloid character of the neutral ground state is weaker as previously predicted via BS DFT, or wavefunction MR and coupled-clusters theories, though present.<sup>[35]</sup>

To further stress the importance of electron correlation and MR effects in the description of multiple charged wavefunctions in ladder-type systems, and to strengthen the BS-UDFT based approach, we performed a fractional occupation electron density (FOD) analysis for some BBL oligomers in their neutral, polaron ( $q = \pm 1e$ ), and bipolaron ( $q = \pm 2e$ ) states. As introduced by Grimme and Hansen,<sup>[36]</sup> FOD is a tool to gauge the MR character of a compound.<sup>[37]</sup> FOD number ( $N_{\text{FOD}}$ ) is a measure of how many highly correlated electrons are in the system. The larger is  $N_{\text{FOD}}$  the higher is the MR character of the system. As a consequence, in the context of HF or DFT approaches, the presence of BS solutions might appear.

Table S1 of the Supporting Information collects the computed  $N_{\text{FODs}}$  for neutral, polaron, and bipolaron states of few BBL oligomers. Notably, each electronic state shows high  $N_{\text{FOD}}$  values ( $\geq 0.7$ ), which increase by lengthening the chain. The trend confirms a not negligible contribution from SEC in the description of the electronic wavefunction. The high  $N_{\text{FODs}}$  for the neutral state (Table S1, Figures S1 and S2, Supporting Information) already indicate a pronounced polyradical character of BBL.<sup>[28]</sup> Charged states, P $\pm$ (S) and B $\pm$ (D) show higher  $N_{\text{FODs}}$  than the neutral species, with values for holes larger than electrons. The FOD analysis justifies the presence of BS solutions,<sup>[38]</sup> for BBL charged species (Figure 1), pointing out the role of SEC/MR effects in determining the electronic wavefunction of charged states.

To explicitly take into account MR effects and to prove their contributions in shaping the charged state electronic wavefunctions, we performed CASSCF/NEVPT2 calculations on a reference system, namely BBL monomer unit. Results are detailed in the Supporting Information. CASSCF wavefunction for BBL1 B+(S) undoubtedly indicate a strong contribution of doubly excited determinants (i.e., H,H  $\rightarrow$  L,L – with H the highest occupied molecular orbital and L lowest one) in the description of the ground state ( $\approx 40\%$ ).

FOD and CASSCF/NEVPT2 calculations corroborate the BS-UDFT analysis for describing the multiple charged states of BBL, highlighting the importance of SEC effects in casting the electronic wavefunction of both electron and hole polarons and bipolarons. BS-UDFT solutions (when found) can represent an effective approximation to describe the complex MR/polyradicaloid electronic structures of redox states in large conjugated systems. Such aspect is particularly valid for BBL, though we believe it is generally true for the whole class of LCPs.

To understand the relaxation and spatial confinements<sup>[39]</sup> of electron versus hole polarons and bipolarons along with the polymer ladder chain, we compared the computed spin densities in Figure 2. A long oligomer, i.e., BBL5 as representative of the polymer, is considered. Both electron and hole polarons localize over a portion of the chain. Such aspect is a physical property of the system, the reason why can be traced back to the localized nature of the molecular orbitals as described at the DFT BS level.

While electron P-(D) localizes over the benzophenanthroline conjugated segment, hole P+(D) localizes over the benzimidazole moiety (Figure 2), leading to different structural and charge relaxations. In particular, for P+(D) the spin density is localized around the imide units. Such different relaxations between electron and hole lead to different response properties, as discussed infra. Bipolaron states relax over two spatial separated chain segments, for both electrons and holes. The B $\pm$ (S) spin densities reflect the radical character of bipolaron singlet state wavefunction. Bipolaron triplet states B $\pm$ (T) relax over the same conjugated segments as B $\pm$ (S) do.

The presence of heterogroups, such as carbonyls and imides, localize the polaron defects,<sup>[40]</sup> favoring the confinement of the structural deformations and spin densities upon charging. We speculate that other LCPs might show BS DFT solutions for both neutral and charged states, therefore localized structural/



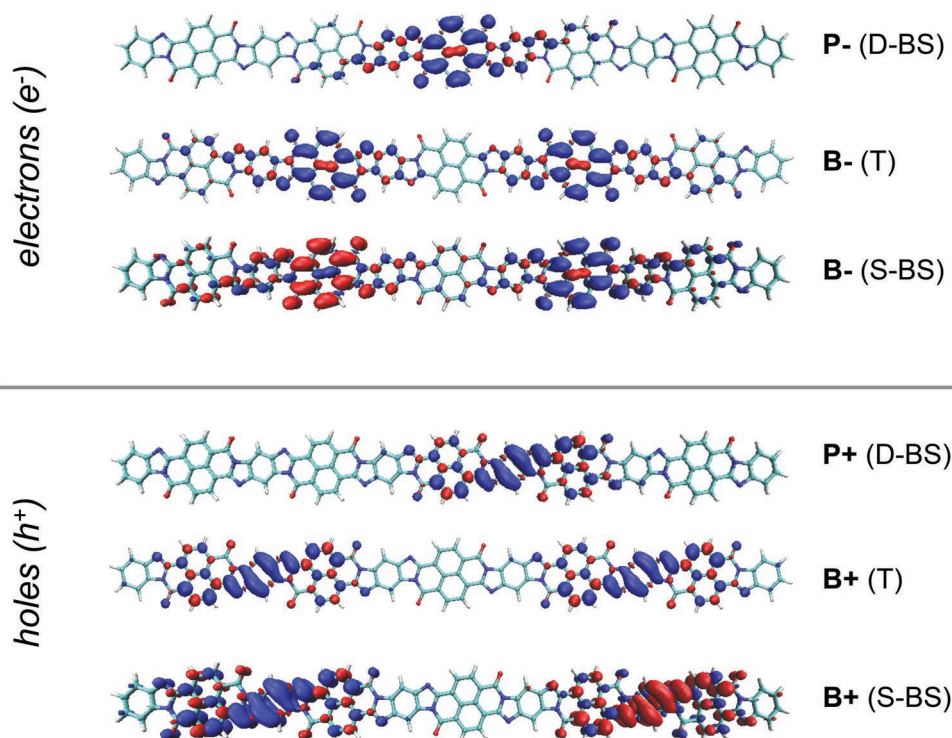


**Figure 2.** Electrons (top) and holes (bottom) spin densities ( $\rho$ ) calculated at the BS-UDFT level of theory ( $\omega$ B97X-D/6-31G\*), for polarons doublet (P(D)), bipolaron singlet (B(S)), and UDFT for bipolaron triplet (B(T)) states. Spin densities were calculated as  $\rho = (\rho^\alpha - \rho^\beta)$  at isovalues of 0.001 Å<sup>3</sup>. Data refer to BBL5 *trans*.

spin density relaxations. We believe this is a general characteristic of LCPs, given their ladder structure and high  $\pi$ -electron delocalization, resulting in not negligible long-range electron correlations and MR/polyradical effects.<sup>[26b]</sup> However, the chain length at which the MR/polyradical character become prominent has to be carefully evaluated for each polymer case, and moreover it should be benchmarked over a wide variety of methods.<sup>[30]</sup>

## 2.2. Electronic Structure of BBL Multiple Negatively Charged States

Multiple negatively charged species cover a crucial role in understanding the variety of redox and charge transport processes occurring in BBL upon charging,<sup>[13,14,20b,41]</sup> as documented in the introduction. Upon reduction BBL shows two insulator-to-conductor transitions, having two conductive states (high, conductive state I:  $9 \times 10^3$  S cm<sup>-1</sup>, and low, conductive state II:  $1.5 \times 10^3$  S cm<sup>-1</sup>) and two insulating states. Sariciftci and co-workers tentatively assigned the multiple redox states to four species proposing the following multiple-charging reduction scheme:<sup>[14]</sup>

- BBL (pristine, insulator) +  $q_a = \text{BBL}^{q_a}$  (species A, conductive state I)
- $\text{BBL}^{q_a} + q_b = \text{BBL}^{(q_a+q_b)}$  (species B, insulating state I)
- $\text{BBL}^{(q_a+q_b)} + q_c = \text{BBL}^{(q_a+q_b+q_c)}$  (species C, conductive state II)
- $\text{BBL}^{(q_a+q_b+q_c)} + q_d = \text{BBL}^{(q_a+q_b+q_c+q_d)}$  (species D, insulating state II)

The total consumed electron per repeat unit (eru) was measured as one ( $q_a + q_b + q_c + q_d = 1$  eru), and the partial charges transferred at different stages were determined as:  $q_a = 0.25$  eru,  $q_b = 0.25$  eru,  $q_c = 0.35$  eru, and  $q_d = 0.15$  eru. In such frame, the high conductive state I was referred to species A (0.25 eru), while the low conductive state II as species C (0.85 eru). The two insulating states were related to species B (0.50 eru) and D (1 eru), respectively.

To model such electron charging scheme, we considered the BBL4 oligomer, both *cis* and *trans* conformers, as a model system. In Figure 3 are reported the energies of each multiple charged state (panel a) together with the relative spin densities (panel b). The correlation between the experimental redox species (A, B, C, D) and the charged states we modeled, is as follows: species A corresponds to a total charge for BBL4 of  $q = 1e^-$  (i.e., P-(D)) leading to 0.25 eru, species B to  $q = 2e^-$  (i.e., B-(S)/B-(T)) giving 0.50 eru, species C to  $q = 3e^-$  (state multiplicities D or Q) corresponding to 0.75 eru, and species D to  $q = 4e^-$  (state multiplicities Qui, T or S) with 1 eru. We assumed that the experimental species C (measured as 0.85 eru) can be approximated to the case of  $q = 3e^-$ , therefore 0.75 eru.

BS solutions are indicated in Figure 3, together with the state spin multiplicity. Notably, almost each state shows a BS solution, remarking the role played by SEC and MR effects in governing the electronic wavefunction of such multiple negatively charged states. In BBL4 *cis*, upon charging the energies of all electronic states fall within the thermal activation energy at room temperature ( $k_B T \approx 25$  meV). For the case of bipolaron, singlet and triplet states, B-(S) and B-(T), are almost degenerate, leading

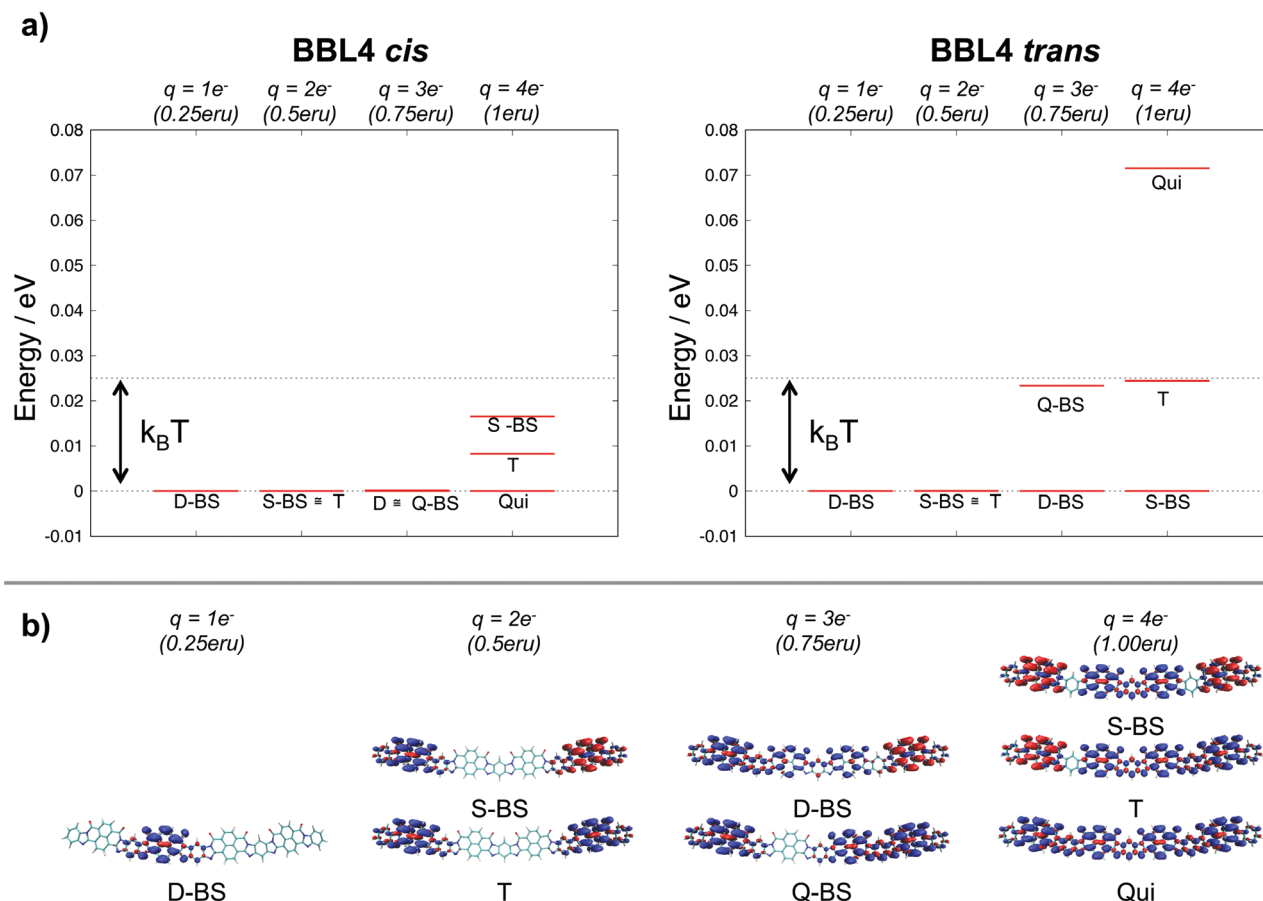


**Figure 3.** Top panels: calculated energy difference for electronic negatively charged states for BBL4 *cis*, as defined by the total charge  $q$ . Polaron,  $q = 1e^-$ , doublet (D). Bipolaron,  $q = 2e^-$ , singlet (S) or triplet (T).  $q = 3e^-$ , doublet (D) or quadruplet (Q).  $q = 4e^-$ , quintet (Qui), triplet (T) or singlet (S). Broken-symmetry (BS) solutions are indicated, when found. Total negative charges per BBL4, correspond to eru, namely:  $q = 1e^-$  (0.25 eru),  $q = 2e^-$  (0.50 eru),  $q = 3e^-$  (0.75 eru), and  $q = 4e^-$  (1 eru). Both *cis* (left) and *trans* (right) conformers are reported. Bottom panel: computed spin densities for each negative charged state. Level of theory ( $\omega$ B97X-D/6-31G\*).).

to a  $\Delta E(S-T)$  very small ( $|\Delta E| \approx 0.008$  eV). The same holds for  $q = 3e^-$  (i.e., 0.75 eru), with doublet and quartet states degenerate, and for  $q = 4e^-$  (1 eru), with quintet, triplet and singlet states within  $k_B T$ . BBL4 *trans* slightly differs from *cis*, however all electronic negatively charged states reside below 0.08 eV of energy difference.

These findings highlight a remarkable aspect of BBL: multiple redox states show a variety of spin state multiplicities (e.g., singlet, doublet, triplet, quadruplet, quintet, etc.), and all states (for a given charge) reside within an energy difference of the order of  $k_B T$  (or  $<0.1$  eV). Therefore, for a given redox species, multiple states with different spin multiplicities can become equally accessible and populated by thermal activation. The energetic scenario draw in Figure 3 underlies the complex and multifaceted redox behaviour of BBL upon electron doping.

The analysis of the spin densities, is reported in panel b, Figure 3. Similarly to BBL5 (Figure 2), we can recognize that also for BBL4 electron P-(D) is mainly localized over a unit, and bipolarons B-(S) and B-(T) are localized over two. The cases of  $q = 3e^-$  (0.75 eru) and  $4e^-$  (1 eru) show localization over three and four units, respectively.

Given the low energy differences between states and the expected DFT energy error, we can say that states with the highest spin multiplicity usually feature the lowest energy. Notably, multiple charged states show a localized character, highlighting the polaronic nature of such redox species.

### 2.3. IR Vibrational Spectra of BBL Polaron, Bipolaron, and Multiple Charged Species

Based on such model system, given the energies and spin multiplicities by checking the existence of BS-UDFT solutions, we were finally able to assign the redox species as those observed in the experiments by Wilbourn and Murray,<sup>[10]</sup> and Sariciftci and co-workers,<sup>[14]</sup> by computing the vibrational and electronic spectra.

In Figure 4 are shown the computed IR spectra for each multiple (negative) charged states with respect to the experimental FT-IR spectroelectrochemical measurements.<sup>[14]</sup>

The electron polaron P-(D) for both *cis* and *trans* conformers, shows four peculiar IRAV bands<sup>[42]</sup> in the spectral regions 1650,

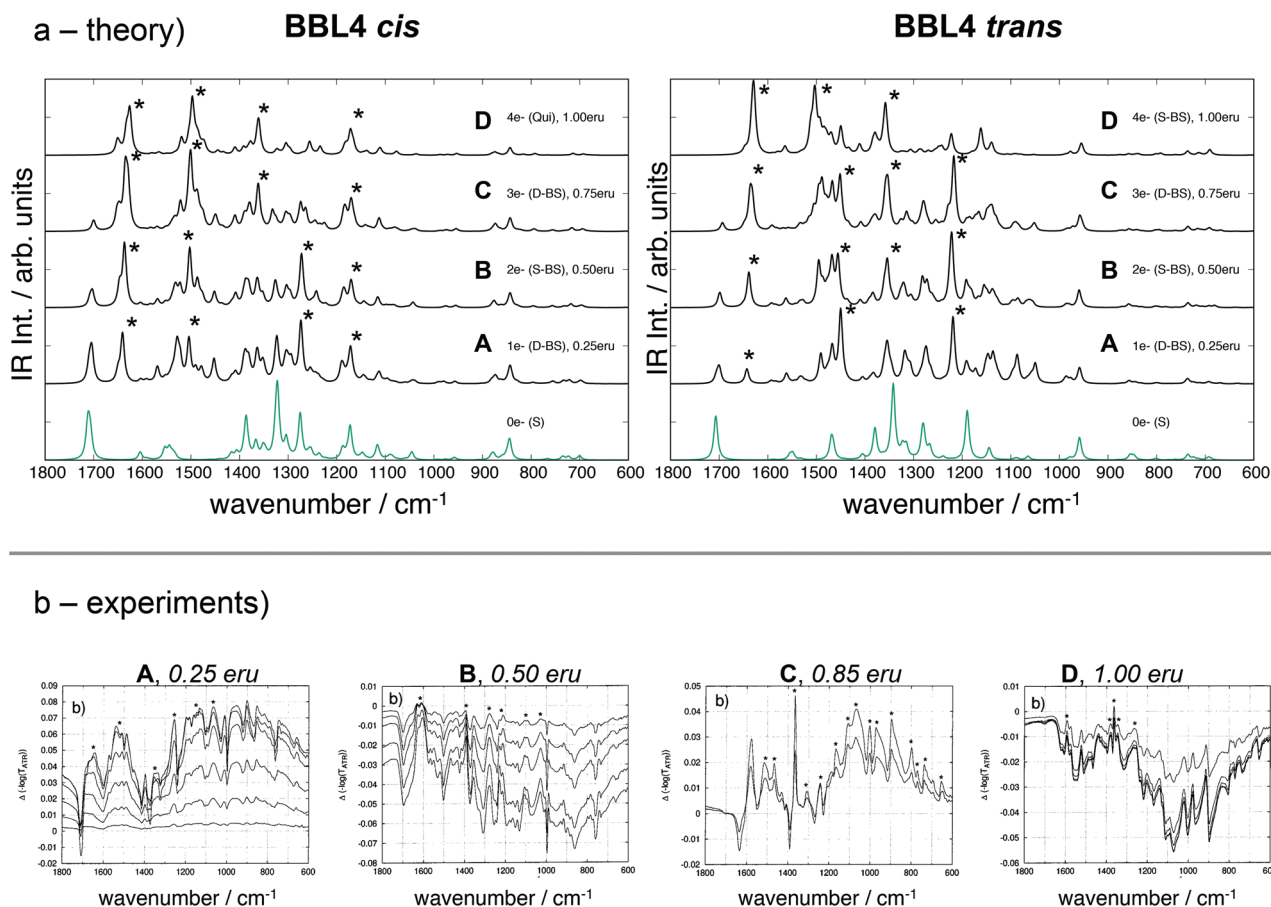


**Figure 4.** Top panel: theoretical IR spectra for BBL4 *cis* (left) and *trans* (right) computed for neutral (green line) and different negative charged states, namely,  $q = 1e^-$  (0.25 eru) species A,  $q = 2e^-$  (0.50 eru) species B,  $q = 3e^-$  (0.75 eru) species C, and  $q = 4e^-$  (1 eru) species D. Labels \* mark relevant IR active modes. Computed frequencies ( $\omega_{B97X-D/6-31G^*}$ ) were rescaled by a scaling factor 0.93 to match experimental data. Bottom panel: experimental FT-IR spectroelectrochemistry data. Reproduced and readapted with permission.<sup>[14]</sup> Copyright 2019, ACS. Redox species A (0.25 eru), B (0.50 eru), C (0.85 eru), and D (1 eru).

1500, 1280, and 1200  $\text{cm}^{-1}$  (labeled with \* in Figure 4; also see Supporting Information for a spectroscopic assignment). The 1650  $\text{cm}^{-1}$  band is associated with the antisymmetric stretching mode of the two carbonyl groups involved in the polaron structural relaxation (see spin density map, Figure 3). The intensity of such band is higher for the *cis* than the *trans*, given the different directionalities of the carbonyl groups. Another intense IR active band is located around 1280–1300  $\text{cm}^{-1}$  being related to the CN stretching coupled with the CH rocking mode.

The computed IR spectra well reproduce the experimental one (despite the high signal-to-noise ratio of the latter),<sup>[14]</sup> and allowed us to assign the high conductive state I, species A (0.25 eru), to the electron polaron P–(D) state.

The IR spectra of bipolarons show a red shift of the 1650  $\text{cm}^{-1}$  band for both *cis* and *trans* conformers (toward 1635  $\text{cm}^{-1}$ ). Such band represents the antisymmetric stretching of the carbonyl groups belonging to the two repeat units where the bipolaron is localized (see spin density map, Figure 3). To note, it is also the global intensification of all bands in the regions 1600, 1500, and 1300  $\text{cm}^{-1}$ . For the case of BBL *trans* we can observe a gradual intensification of the band around 1350  $\text{cm}^{-1}$  (see Figure 4). Good agreement with the experimental data (see Sup-

porting Information) is observed, allowing us to refer species B (0.50 eru), i.e., the insulator state, as the electron bipolaron. Very little differences can be seen by comparing the computed IR spectra for singlet B–(S) and triplet B–(T) bipolarons (see Supporting Information).

Upon extra charging, toward  $q = 3e^-$  and  $4e^-$ , with 0.75 and 1 eru, respectively, the computed IR spectra change as follows: i) a gradual red shift of the 1650  $\text{cm}^{-1}$  band toward 1600  $\text{cm}^{-1}$ , and ii) an intensification of the IR bands around 1500 and 1400–1350  $\text{cm}^{-1}$  regions. We can assign the calculated IR bands to the experimental ones observed for species C and D (see Supporting Information), therefore referring species C (conductive state II) to the charging case of  $q = 3e^-$ , and species D (insulator state II) to  $q = 4e^-$ . Differences between the computed IR spectra for each state spin multiplicity are very minor and reported in the Supporting Information.

At the current stage it is difficult to discriminate between *cis* and *trans* conformers by comparing the calculated versus experimental IR spectra. Experimentally samples are not pure *cis* or *trans* isomers, every chain containing a statistical distribution of both by virtue of the condensation polymerization method used.<sup>[1b]</sup> Even though the detailed spectroscopic assignment will

be the subject of another study, we can already observe some specific vibrational fingerprints.

For redox species A, the intense IR band at  $1650\text{ cm}^{-1}$  and the spectral shape around  $1500\text{ cm}^{-1}$  can be better assigned to conformer *cis*. For the redox species C i) the sharp intense band around  $1400\text{ cm}^{-1}$  in the experimental data (here assigned to a quinoidal mode on a benzophenanthroline unit coupled with the CN stretching) can be attributed to the *trans* conformer, and ii) the two intense experimental bands around  $1500\text{ cm}^{-1}$  region can be interpreted as a superposition of bands belonging to both *cis* and *trans*. For redox species D, we can recognize the IR bands at  $1600\text{ cm}^{-1}$  for both BBL *cis* and *trans*, together with the intense band at  $1350\text{ cm}^{-1}$ .

The good correlation between the theoretical and experimental data directly validates our BS DFT approach in describing the electronic structure and response properties of multiple charged states in LCPs.<sup>[24]</sup> Moreover, we were able to assign for the first time all redox species (A, B, C, D) as previously identified experimentally,<sup>[14]</sup> however never characterized.

Summarizing, we can refer the high conductive state I (species A) to the electron P–(D) doublet state, and the low conductive state II (species C) to the case with a total charge  $q = 3e^-$  for BBL4, i.e., 0.75 eru, being either a doublet or a quartet electronic state (Figure 3). The two insulating states can be assigned to bipolarons (either B–(S) or B–(T)), and to a state with a total charge  $q = 4e^-$  for BBL4 (i.e., 1 eru) showing either quintet, triplet or singlet state multiplicity (Figure 3).

Given the current experimental data-set available in literature,<sup>[14]</sup> it is difficult to discriminate amongst different BBL conformers and state multiplicities playing during the multi-electron doping processes. Further experimental data, such as electron spin resonance spectroscopy, would be required.

## 2.4. Electronic Spectra of BBL Polaron, Bipolaron, and Multiple Charged Species

A possible way to get insights into the nature of multiple redox states upon electron doping, can be by analysing the electronic transitions of charged species.

In Figure 5 is reported the comparison between the computed vertical electronic transitions, for each multiple charged state, between BBL *cis* and *trans*. It can be noted that the comparison BBL *cis* versus *trans* leads to markedly different elec-

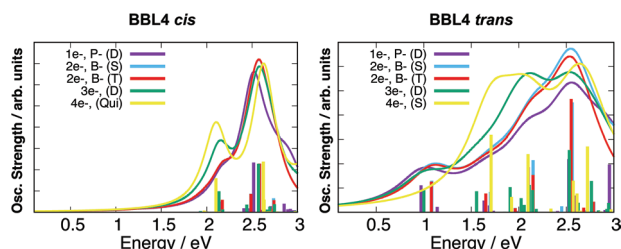


**Figure 5.** Computed electronic vertical transition energies (unscaled values) at the time-dependent TD-DFT ( $\omega$ B97X-D/6-31G\*) for electron polaron (P(D)), bipolaron (B(S), B(T)),  $q = 3e^-$  (doublet, D), and  $q = 4e^-$  (quintet or singlet) states. BBL4 *cis* (left) and *trans* (right) conformers are reported. Spectra were obtained as convolution of Lorentzian functions.

tronic spectroscopic responses. The excitation energies of BBL *trans* for the polaron ( $q = 1e^-$ ), bipolaron ( $q = 2e^-$ ),  $q = 3e^-$ , and  $q = 4e^-$  are generally lower in energy, showing broader spectra, than the *cis*. The negatively charged species of BBL *trans* show dipole active excited states in the mid-IR region, while for BBL *cis* such low-energy excited states, though present, are optically forbidden (or with negligible oscillator strength, see Supporting Information).

While polaron and bipolaron show similar electronic transitions, within each conformer, the case for  $q = 3e^-$  (0.75 eru) and  $4e^-$  (1 eru) differ, leading to more intense oscillator strengths and broader absorption bands.

Spectroelectrochemical data reported by Wilbourn and Murray,<sup>[10]</sup> and recent UV–vis spectra recorded upon electron chemical doping,<sup>[18,20b]</sup> well match the theoretical predictions of the excited state for the P–(D) species. Wilbourn and Murray<sup>[10]</sup> also report the UV–vis spectra by changing the reduction potential. Evidences of an enhancement in the band intensities around 2.5–2.3 eV, and further below at 1.3 eV, well match the computed electronic spectra for BBL *trans*, Figure 5. The published data document the presence of an absorption band starting at 900 nm (1.3 eV), which increases its intensity by increasing the redox potential. For the case of BBL *trans*, we indeed predicted low-lying excited states (<1 eV) for both electron polarons and bipolarons.

As reported before for the IR spectra, the active species present in solution or in thin films are most likely a mixture of BBL *cis* and *trans* conformers.

Regardless specific assignments, given the differences in the computed electronic transitions for multiple redox states, we envisage that UV–vis spectroelectrochemistry—around 2–1.5 eV and down to 1.3–0.3 eV spectral regions—can be a valuable tool to discriminate amongst BBL conformers and between different electronic redox states playing upon electron charging, as clearly shown in Figure 5.

## 2.5. Role of Protonation in BBL Neutral and Charged Species

A relevant question still has to be answered in literature regards the effects of protonation, and the mutual presence of protonated and reduced states as induced by doping, in affecting BBL structural and spectroscopic properties.<sup>[8,10]</sup> This aspect is very relevant in the literature of BBL and other LCPs, being such polymers processed by using strong protonic acids to favor their solubility and processability. As a consequence, a fraction of protonated species is inevitably present in the active material, eventually affecting the optoelectronic properties.

Figure 6 compares the computed IR and UV–vis spectra for the following three cases of BBL4 *cis*: a protonated oligomer (1H+ per repeat unit, named 4H+), a charged oligomer with  $q = 4e^-$  (1 eru) and a protonated/charged oligomer (4H+/4e-). The protonated species shows an intense IR band at  $1000\text{ cm}^{-1}$  (see Figure 6). Such transition, associated to the CH rocking coupled with the NH rocking localized on one benzophenanthroline unit, is always present in any IR spectrum of pristine BBL.<sup>[8,14]</sup> On the contrary, as evident from our calculations, such band is not related to a pristine species, rather to a (partially)



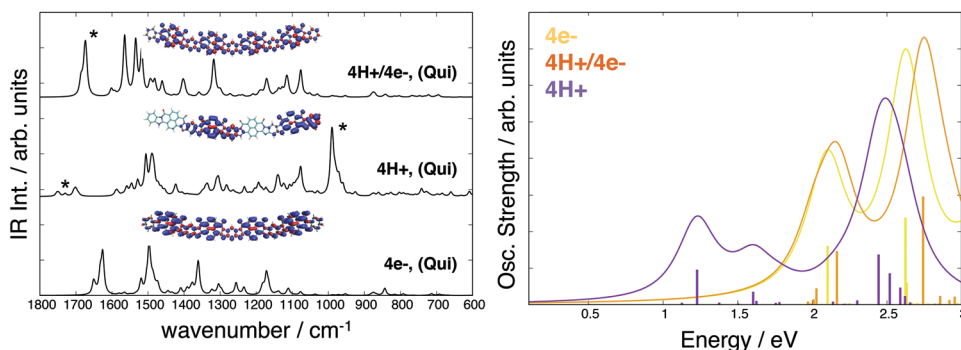


**Figure 6.** Left panel: computed IR spectra (scaling factor 0.93) for BBL4 *cis* protonated (4H+), charged ( $q = 4e^-$ , 1 eru) and protonated/charged (4H+/4e<sup>-</sup>) species (all quintet state multiplicity), together with the spin densities. Right panel: relative computed TD-DFT vertical transition energies (unscaled values).

protonated species. The computed IR spectra of neutral BBL *cis* and *trans* (see Figure 4) in fact do not show any intense IR band around 1000 cm<sup>-1</sup>.

Notably, the intensity of the IR band associated to the protonated species is orders of magnitude higher than the band intensities of the neutral species in the same spectral region. We speculated that even low concentrations of protonated species in *pristine* samples can lead to an intense IR band at 1000 cm<sup>-1</sup>.<sup>[8,14]</sup> To note, it is also the broadening of the IR spectrum of BBL4 protonated species (4H+) in the region of the carbonyl bands (see at 1700 cm<sup>-1</sup> in Figure 6), shifting the frequencies toward high wavenumbers. Such spectral spread was already reported in early experimental data by Kim,<sup>[8]</sup> however never carefully investigated. We can prove that the broadening at 1700 cm<sup>-1</sup> is due to the presence of a protonated species (see Supporting Information).

In Figure 6 are shown also the computed electronic transitions (TDDFT data) for the protonated (4H+), charged ( $q = 4e^-$ , 1 eru) and protonated/charged (4H+/4e<sup>-</sup>) species. The protonated (4H+) species shows a distinctive absorption band around 1.2 eV, leading to a spectrum remarkably different than the charged or protonated/charged species. Such low-energy band is the  $S_0 \rightarrow S_1$  transition, described (see Supporting Information) as single excitations from singly occupied to unoccupied orbitals localized over few units. Unfortunately, we could not find experimental data to corroborate our calculations. We otherwise believe our theoretical spectroscopic predictions may serve as a valuable tool for both theoreticians and experimentalists to characterize the multiple redox and protonated species of BBL, present in solution or solid state.<sup>[10]</sup> Spin densities for each protonated and charged case are reported as insets in Figure 6 too, showing the localization of the spins, therefore the polaronic nature of such multiple redox/protonated species.

### 3. Conclusion

LCPs gained a renewed interest owing to their remarkable chemical, mechanical, optoelectronic, and energy-conversion properties. Amongst LCPs, BBL is the most investigated one, showing the highest electron mobility (0.1 cm<sup>2</sup> V<sup>-1</sup> s<sup>-1</sup>), electrical conductivity (1.7 S cm<sup>-1</sup>), and thermoelectric power

factor (0.43 μW m<sup>-1</sup> K<sup>-2</sup>). Such outstanding figures-of-merit are achieved via (electro)-chemical doping, leading to a series of multiple redox states whose structural, electronic, and optical responses have never been comprehensively rationalised. Despite the numerous reports on BBL, the understanding of fundamental electronic and chemical–physical properties remains poor. We filled such knowledge-gap through an extended quantum-chemical investigation modeling the multiple charged states of BBL, assessing their structural, spin, and spectroscopic properties, ultimately comparing our data with the available experimental results.

We found that the electronic wavefunction of charged states (e.g., polarons, bipolarons, and multiple redox states) shows remarkable electron correlation effects and multiconfigurational characters, features that we addressed via a combined use of BS-UDFT and FOD calculations, as well supported by MR wavefunction methods.

Holes (i.e., oxidized species) showed higher MR/radicaloid character than electrons (reduced species). MR wavefunction calculations corroborated such aspect, reporting a strong contribution of double excitations in the description of the BBL ground state hole bipolaron wavefunction.

Comparing the electron and the hole states, we found that the structural and spin-density relaxations of polaron, bipolaron, and multiple redox states showed distinctive differences. Electrons relax upon the benzophenanthroline segments, while holes localize over the benzimidazole moieties. Both polarons are spatially localized, allowing BBL to host multiple charges, a property that can be exploited for thermoelectric and electrode-battery applications.

Upon electrochemical doping BBL shows multiple conductive regimes, leading to two insulator-to-conductor transitions, as reported in literature. We modeled such complex redox scenario by mimicking the multiple charged states of BBL up to 1 eru. We found a variety of spin state multiplicities (e.g., singlet, doublet, triplet, quartet, quintet, etc.) by varying the charge accommodated on the chain, revealing a wide range of quasidegenerate electronic states all lying within  $k_B T$ , or below 0.1 eV. Notably, given a certain charge, states with different spin multiplicities can be thermally populated.

The multiple redox states can be represented as follows: the polaron as 0.25 eru ( $q = 1e^-$ ), the bipolaron as 0.50 eru ( $q = 2e^-$ ),

and the multiple redox states as 0.75 eru ( $q = 3e^-$ ) and 1 eru ( $q = 4e^-$ ).

We were able to assign the conductive/insulating regimes observed in literature to specific multiple charged states of BBL, by comparing the computed IR vibrational spectra to the experimental ones. We found that the high conductive state I can be related to the polaron (doublet), the low conductive state II to the redox species with 0.75 eru (being either doublet or quartet), the two insulating states to the bipolaron (either singlet or triplet), and to the redox case with 1 eru (either quintet, triplet or singlet).

Furthermore, we assigned the main intense IRAV bands of the polaronic species to the antisymmetric stretching of the carbonyl groups ( $1650\text{ cm}^{-1}$ ). A blue shift of such band is predicted passing from polaron (0.25 eru), bipolaron (0.50 eru), and up to 1 eru charged state. This clear assignment would allow future experimental and quantitative monitoring of the doping levels and conductive species upon doping.

We evaluated the electronic transitions of multiple redox states, finding that BBL *cis* and *trans* conformers show remarkable variations in the excited states. The latter shows low-energy optical allowed transitions, otherwise not active in the *cis*.

Finally, we addressed the role of protonation in BBL. Protons, localized on the imide units, induce a polaron-like spin density. A peculiar vibrational signature of protonated species is the intense IR band at  $1000\text{ cm}^{-1}$ . Moreover, protonated species shows a distinctive electronic absorption band, leading to an absorption spectrum remarkably different than the charged or protonated/charged cases.

Our modeling of multiple charged BBL species reconciles contradictory experimental and computational observations, shedding light onto the polaronic structure–property functions of BBL, so far the most prominent polymer amongst LCPs in the field of organic electronics.

## 4. Experimental Section

Detailed information concerning each aspect of the quantum-chemical calculations is reported in the Supporting Information.

## Supporting Information

Supporting Information is available from the Wiley Online Library or from the author.

## Acknowledgements

D.F. acknowledges the Deutsche Forschungsgemeinschaft (DFG) for a grant (FA 1502/1-1 “Molecular Understanding of Thermo-Electric Properties in Organic Polymers”) and the Regional Computing Centre (RRZK) of Universitaet zu Koeln, for providing computing time and resources on the HPC RRZK CHEOPS. F.N. acknowledges the financial support of University of Bologna (RFO). Correction added on 21 January 2021, after first online publication: Projekt Deal funding statement has been added.

Open access funding enabled and organized by Projekt DEAL.

## Conflict of Interest

The authors declare no conflict of interest.

## Keywords

broken-symmetry density functional theory, doping, ladder-type polymers, polarons, radicaloids, redox species

Received: July 31, 2020

Revised: November 6, 2020

Published online: December 4, 2020

- [1] a) J. Lee, A. J. Kalin, T. Yuan, M. Al-Hashimi, L. Fang, *Chem. Sci.* **2017**, *8*, 2503; b) U. Scherf, *J. Mater. Chem.* **1999**, *9*, 1853; c) R. S. Sprick, A. Thomas, U. Scherf, *Polym. Chem.* **2010**, *1*, 283; d) E. Khodabakhshi, C. Ramanan, J. J. Michels, S. Bonus, D. Hertel, K. Meerholz, M. Forster, U. Scherf, P. W. M. Blom, *Adv. Electron. Mater.* **2020**, *6*, 2000082; e) R. Lu, Y. Han, W. Zhang, X. Zhu, Z. Fei, T. Hodsdon, T. D. Anthopoulos, M. Heeney, *J. Mater. Chem. C* **2018**, *6*, 2004; f) I. Belaish, D. Davidov, H. Selig, M. R. McLean, L. R. Dalton, *Adv. Mater.* **1989**, *11*, 387; g) W. Graupner, J. Partee, J. Shinar, G. Leising, U. Scherf, *Phys. Rev. Lett.* **1996**, *77*, 2033.
- [2] A.-D. Schlüter, *Adv. Mater.* **1991**, *3*, 282.
- [3] Y. Yin, S. Zhang, D. Chen, F. Guo, G. Yu, L. Zhao, Y. Zhang, *Polym. Chem.* **2018**, *9*, 2227.
- [4] R. L. V. Deusen, *Polym. Lett.* **1966**, *4*, 211.
- [5] L. Yu, M. Chen, L. R. Dalton, *Chem. Mater.* **1990**, *2*, 649.
- [6] a) A. Vogel, M. Forster, L. Wilbraham, C. L. Smith, A. J. Cowan, M. A. Zwiijnenburg, R. S. Sprick, A. I. Cooper, *Faraday Discuss.* **2019**, *215*, 84; b) J. Lee, B. B. Rajeeva, T. Yuan, Z. H. Guo, Y. H. Lin, M. Al-Hashimi, Y. Zheng, L. Fang, *Chem. Sci.* **2016**, *7*, 881; c) Y. Chen, H. Li, M. Tang, S. Zhuo, Y. Wu, E. Wang, S. Wang, C. Wang, W. Hu, *J. Mater. Chem. A* **2019**, *7*, 20891.
- [7] H. Sibirakawa, E. J. Louis, A. G. MacDiarmid, C. K. Chiang, A. J. Heeger, *J. Chem. Soc., Chem. Commun.* **1977**, 578.
- [8] O.-K. Kim, *J. Polym. Sci., Polym. Lett. Ed.* **1982**, *20*, 663.
- [9] O.-K. Kim, *Mol. Cryst. Liq. Cryst.* **1984**, *105*, 161.
- [10] K. Wilbourn, R. W. Murray, *Macromolecules* **1988**, *21*, 89.
- [11] T. Zheng, F. Badrun, I. M. Brown, D. J. Leopold, T. C. Sandreczki, *Synth. Met.* **1999**, *107*, 39.
- [12] T. Yohannes, H. Neugebauer, S. Luzzati, M. Catellani, S. Yi, S. A. Jenekhe, N. S. Sariciftci, *Synth. Met.* **2001**, *119*, 319.
- [13] K. Wilbourn, R. W. Murray, *J. Phys. Chem.* **1988**, *92*, 3642.
- [14] T. Yohannes, H. Neugebauer, S. Luzzati, M. Catellani, S. A. Jenekhe, N. S. Sariciftci, *J. Phys. Chem. B* **2000**, *104*, 9430.
- [15] a) H. Antoniadis, M. A. Abkowitz, J. A. Osaheni, S. A. Jenekhe, M. Stolka, *Chem. Mater.* **1994**, *6*, 63; b) M. M. Alam, S. A. Jenekhe, *J. Phys. Chem. B* **2002**, *106*, 11172.
- [16] a) A. Babel, S. A. Jenekhe, *J. Am. Chem. Soc.* **2003**, *125*, 13656; b) A. L. Briseno, F. S. Kim, A. Babel, Y. Xia, S. A. Jenekhe, *J. Mater. Chem.* **2011**, *21*, 16461; c) H. Sun, J. Gerasimov, M. Berggren, S. Fabiano, *J. Mater. Chem. C* **2018**, *6*, 11778.
- [17] S. A. Jenekhe, S. Yi, *Appl. Phys. Lett.* **2000**, *77*, 2635.
- [18] S. Wang, H. Sun, U. Ail, M. Vagin, P. O. Persson, J. W. Andreasen, W. Thiel, M. Berggren, X. Crispin, D. Fazzi, S. Fabiano, *Adv. Mater.* **2016**, *28*, 10764.
- [19] a) J. Wu, X. Rui, C. Wang, W.-B. Pei, R. Lau, Q. Yan, Q. Zhang, *Adv. Energy Mater.* **2015**, *5*, 1402189; b) J. Xie, W. Chen, Z. Wang, K. C. W. Jie, M. Liu, Q. Zhang, *Chem. Asian J.* **2017**, *12*, 868.
- [20] a) X. L. Chen, S. A. Jenekhe, *Macromolecules* **1997**, *30*, 1728; b) K. Xu, H. Sun, T.-P. Ruoko, G. Wang, R. Kroon, N. B. Kolhe, Y. Puttison,

- X. Liu, D. Fazzi, K. Shibata, C.-Y. Yang, N. Sun, G. Persson, A. B. Yankovich, E. Olsson, H. Yoshida, W. M. Chen, M. Fahlman, M. Kemerink, S. A. Jenekhe, C. Müller, M. Berggren, S. Fabiano, *Nat. Mater.* **2020**, *19*, 738.
- [21] S. Y. Hong, M. Kertesz, Y. S. Lee, O.-K. Kim, *Macromolecules* **1992**, *25*, 5424.
- [22] S. Ghosh, V. Gueskine, M. Berggren, I. V. Zozoulenko, *J. Phys. Chem. C* **2019**, *123*, 15467.
- [23] a) I. Zozoulenko, A. Singh, S. K. Singh, V. Gueskine, X. Crispin, M. Berggren, *ACS Appl. Polym. Mater.* **2019**, *1*, 83; b) J. L. Brédas, G. B. Street, *Acc. Chem. Res.* **1985**, *18*, 309; c) J. Li, G. D'Avino, A. Pershin, D. Jacquemin, I. Duchemin, D. Beljonne, X. Blase, *Phys. Rev. Mater.* **2017**, *1*, 025602.
- [24] a) D. Fazzi, S. Fabiano, T.-P. Ruoko, K. Meerholz, F. Negri, *J. Mater. Chem. C* **2019**, *7*, 12876. b) P. M. Lahti, A. S. Ichimura, J. A. Sanborn, *J. Phys. Chem. A* **2001**, *105*, 251. c) V. Bachler, G. Olbrich, F. Neese, K. Wieghardt, *Inorg. Chem.* **2002**, *41*, 4179. d) L. Noodleman, *J. Chem. Phys.* **1981**, *74*, 5737. e) L. Noodleman, E. R. Davidson, *Chem. Phys.* **1986**, *109*, 131. f) A. A. Ovchinnikov, J. K. Labanowski, *Phys. Rev. A* **1996**, *53*, 3946. g) C. Adamo, V. Barone, A. Bencini, F. Totti, I. Ciofini, *Inorg. Chem.* **1999**, *38*, 1996.
- [25] J. P. Perdew, A. Savin, K. Burke, *Phys. Rev. A* **1995**, *51*, 4531.
- [26] a) S. Wang, D. Fazzi, Y. Puttison, M. J. Jafari, Z. Chen, T. Ederth, J. W. Andreasen, W. M. Chen, A. Facchetti, S. Fabiano, *Chem. Mater.* **2019**, *31*, 3395; b) M. Bendikov, H. M. Duong, K. Starkey, K. N. Houk, E. A. Carter, F. Wudl, *J. Am. Chem. Soc.* **2004**, *126*, 7416.
- [27] S. Yamanaka, T. Kawakami, H. Nagao, K. Yamaguchi, *Chem. Phys. Lett.* **1994**, *231*, 25.
- [28] G. Salvitti, F. Negri, A. J. Perez-Jimenez, E. San-Fabian, D. Casanova, J. C. Sancho-Garcia, *J. Phys. Chem. A* **2020**, *124*, 3590.
- [29] a) J. L. Bao, L. Gagliardi, D. G. Truhlar, *J. Phys. Chem. Lett.* **2018**, *9*, 2353; b) C. M. Marian, A. Heil, M. Kleinschmidt, *WIREs Comput. Mol. Sci.* **2018**, *9*, e1394.
- [30] N. Dupuy, M. Casula, *J. Chem. Phys.* **2018**, *148*, 134112.
- [31] a) F. Neese, *J. Phys. Chem. Solids* **2004**, *65*, 781; b) F. Neese, *Coord. Chem. Rev.* **2009**, *253*, 526.
- [32] D. Fazzi, E. V. Canesi, F. Negri, C. Bertarelli, C. Castiglioni, *Chem. Phys. Chem.* **2010**, *11*, 3685.
- [33] S. Canola, J. Casado, F. Negri, *Phys. Chem. Chem. Phys.* **2018**, *20*, 24227.
- [34] a) M. Casula, C. Attaccalite, S. Sorella, *J. Chem. Phys.* **2004**, *121*, 7110; b) K. Nakano, C. Attaccalite, M. Barborini, L. Capriotti, M. Casula, E. Coccia, M. Dagrada, C. Genovese, Y. Luo, G. Mazzola, A. Zen, S. Sorella, *J. Chem. Phys.* **2020**, *152*, 204121.
- [35] F. Plasser, H. Pašalić, M. H. Gerzabek, F. Libisch, R. Reiter, J. Burgdörfer, T. Müller, R. Shepard, H. Lischka, *Angew. Chem., Int. Ed.* **2013**, *52*, 2581.
- [36] S. Grimme, A. Hansen, *Angew. Chem., Int. Ed.* **2015**, *54*, 12308.
- [37] C. A. Bauer, A. Hansen, S. Grimme, *Chem. - Eur. J.* **2017**, *23*, 6150.
- [38] S. Canola, Y. Dai, F. Negri, *Computation* **2019**, *7*, 68.
- [39] a) I. H. Nayyar, E. R. Batista, S. Tretiak, A. Saxena, D. L. Smith, R. L. Martin, *J. Chem. Theory Comput.* **2013**, *9*, 1144; b) M. Anderson, C. Ramanan, C. Fontanesi, A. Frick, S. Surana, D. Cheyins, M. Furno, T. Keller, S. Allard, U. Scherf, D. Beljonne, G. D'Avino, E. von Hauff, E. Da Como, *Phys. Rev. Mater.* **2017**, *1*, 055604; c) D. Fazzi, M. Caironi, C. Castiglioni, *J. Am. Chem. Soc.* **2011**, *133*, 19056.
- [40] N. A. Deskins, M. Dupuis, *Phys. Rev. B* **2007**, *75*, 195212.
- [41] A. L. Briseno, S. C. B. Mannsfeld, P. J. Shamberger, F. S. Ohuchi, Z. Bao, S. A. Jenekhe, Y. Xia, *Chem. Mater.* **2008**, *20*, 4712.
- [42] a) W. J. Kendrick, M. Jirásek, M. D. Peeks, G. M. Greetham, I. V. Sazanovich, P. M. Donaldson, M. Towrie, A. W. Parker, H. L. Anderson, *Chem. Sci.* **2020**, *11*, 2112; b) S. Kahmann, D. Fazzi, G. J. Matt, W. Thiel, M. A. Loi, C. J. Brabec, *J. Phys. Chem. Lett.* **2016**, *7*, 4438.